RSC Advances

PAPER

View Article Online
View Journal | View Issue

Cite this: *RSC Adv.*, 2015, **5**, 74162

Efficient synthesis of *p*-chlorobenzaldehyde through liquid-phase oxidation of *p*-chlorotoluene using manganese-containing ZSM-5 as catalyst

Wei-Fang Zhou,[a] Lang Chen,[a] Jun Xie,[a] Chak-Tong Au[ab] and Shuang-Feng Yin*[a]

Received 12th August 2015
Accepted 20th August 2015

DOI: 10.1039/c5ra16206h

www.rsc.org/advances

Manganese-containing MFI-type Mn–ZSM-5 zeolites were prepared and characterized by XRD, UV-vis DRS, SEM, XPS, N_2 adsorption–desorption, NH_3-TPD and ICP-AES techniques. The zeolites show high catalytic activity and selectivity in the heterogeneous oxidation of *p*-chlorotoluene to *p*-chlorobenzaldehyde. The effects of catalyst concentration, water addition, HBr amount, as well as reaction time and temperature on product yield were investigated. Under the optimized conditions (catalyst 20 mg, *p*-chlorotoluene 1 mL, solvent (acetic acid) 10 mL, HBr (40 wt%) 30 mg, H_2O 3 g, oxygen flow rate 50 mL min^{-1}, time 8 h, temperature 100 °C), the Mn–ZSM-5 (Si/Mn = 48, Mn 1.7 wt%) catalyst shows *p*-chlorotoluene conversion of 93.8% and *p*-chlorobenzaldehyde selectivity of 90.5%. The excellent catalytic activity can be attributed to the distribution of Mn species and the mild acid sites.

1. Introduction

As an important intermediate in the production of dyes, pharmaceutical drugs, optical brighteners and agricultural chemicals,[1] *p*-chlorobenzaldehyde (PCB) is manufactured on an industrial scale by side-chain chlorination of *p*-chlorotoluene (PCT) followed by acid hydrolysis using soluble acetates of transition metals as catalysts.[2] The process, however, suffers from low conversion and poor selectivity, and with the use of soluble catalysts, it is hard to be environmentally-benign.[3] Thus, research efforts were employed to investigate the use of solid catalysts.[4]

To be commercially viable, the process for oxidation of aromatic hydrocarbons by molecular oxygen or hydrogen peroxide has to be highly selective.[5] In the last decades, there were formulations for PCT oxidation using heterogeneous catalysts.[3,4,6] For example, Bautista *et al.* reported 19% PCT conversion and 70% PCB selectivity with aqueous H_2O_2 over vanadium oxide catalysts supported on TiO_2–sepiolite.[4] On the other hand, Yoo reported 28% PCT conversion and 61.6% PCB selectivity over Fe/Mo/borosilicate molecular sieves in the presence of O_2.[6] In addition, Wang *et al.* achieved PCB yield of 48.5% with aqueous H_2O_2 over cobalt-doped mesoporous titania.[3] Nevertheless, those approaches are unsatisfactory either in conversion or in selectivity. It is therefore necessary to design solid catalysts active enough for the oxidation reaction.

With micropores close to the molecular diameter of many desired products, zeolites are used as shape-selective catalysts.[7,8] It is known that the Mobil Fifth (MFI)-type ZSM-5 zeolites are unique because their three-dimensional microporous channels are accessible only for molecules that are within 0.6 nm in diameter.[9,10] There are reports on the selective adsorption of benzene and *p*-substituted benzenes over that of *o*- and *m*-substituted aromatic products on nano-sized ZSM-5 catalysts.[11–13] As reported, ZSM-5 zeolites modified with manganese show attractive properties and reactivity.[14–18] Excellent catalytic performance is ascribed to the well-isolated Mn species in the zeolite framework or those anchored on the surface.[17] In addition, oxygen can be easily adsorbed on the defective sites and strongly bound to the manganese centres that are active for selective oxidation.[16] Previously, we synthesized a series of manganese oxide octahedral molecular sieves that show excellent catalytic performance towards the oxidation of PCT for the formation of PCB.[19–21] Lately we extended our investigation to the use of supports that have manganese active sites, and explored the relationship between PCB selectivity and the distribution of active sites.

In this article, we report for the first time the liquid-phase catalytic oxidation of PCT (O_2 as oxidant) to PCB in a reflux system using hydrogen bromide as reaction initiator (Scheme 1) over manganese-containing ZSM-5. They are Mn–ZSM-5 (Si/Mn = 48, Mn 1.7 wt%) prepared by a hydrothermal method and Mn/ZSM-5 prepared by an impregnation method. The former shows better activity (93.8%) and selectivity (90.5%) than the latter. As revealed by XRD, UV-vis DRS, SEM, XPS, N_2 adsorption–desorption, NH_3-TPD and ICP-AES analysis, the catalytic performance is significantly influenced by specific surface area, distribution of active sites and mild acid sites.

[a]*Hunan University, College of Chemistry and Chemical Engineering, Changsha, Hunan, China. E-mail: sf_yin@hnu.edu.cn*

[b]*Hong Kong Baptist University, Chemistry, Waterloo Road, Kowloon Tong, Kowloon, Hong Kong, China*

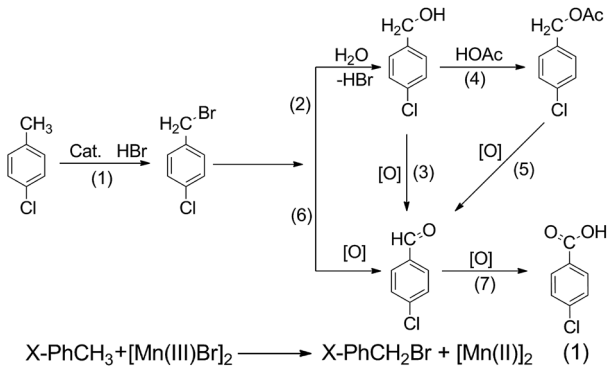

Scheme 1 Liquid-phase catalytic oxidation of *p*-chlorotoluene with O_2 over Mn–ZSM-5.[22]

2. Experimental

2.1. Materials

The chemical reagents were of analytical grade and were used without further purification. No impurities were found in *p*-chlorotoluene by GC analysis. Pure gaseous O_2 was used as the oxygen source.

2.2. Catalysts preparation

All silica ZSM-5 zeolite was prepared by hydrothermal synthesis using tetraethylorthosilicate (TEOS, Aldrich, 98%) as a silicon source and TPAOH (25 wt%) aqueous solution as a structure-directing agent.[23] Typically, 12.5 g of TEOS, 12.5 g distilled water, and 12.4 g aqueous TPAOH (25 wt%) were sequentially added and adequately mixed. The well-mixed solution (solution A) was stirred for 3 h. Then the synthesis was carried out in an autoclave with a Teflon liner at 180 °C for 2 days. The obtained gel was filtered out and washed exhaustively with distilled water, dried overnight at 120 °C and then calcined in air at 550 °C for 5 h. The Mn–ZSM-5 zeolite was synthesized by adding manganese(III)–acetylacetonate (Sigma Aldrich) to solution A.[18] The prepared catalysts are denoted hereinafter as M–Z (*x*), where *x* means the Si/Mn molar ratio.

Mn/ZSM-5 was prepared by impregnation. An appropriate amount of manganese(III)–acetylacetonate precursor was dissolved in deionized water and mixed with 2 g ZSM-5 at 80 °C under magnetic stirring for 4 h. The as-synthesized sample was dried overnight at 120 °C and calcined in air at 550 °C for 5 h. The final product is denoted hereinafter as M/Z (*y*), where *y* stands for the weight percentage of Mn in terms of the whole catalyst.

2.3. Catalyst characterization

The powder X-ray diffraction (XRD) experiment was conducted on a Bruker D8 Advance diffractometer using Cu Kα radiation. The data were recorded at a scan rate of 0.02° (2) s^{-1} in the 10–80° range. UV-vis diffuse reflectance spectra (UV-vis DRS) of samples were obtained over a UV-vis spectrophotometer (Cary 100) using $BaSO_4$ as reference. Scanning electron microscopy (SEM) images were taken on a Hitachi S-4800 emission scanning microscope with a Schottky emitter at an accelerating voltage of 5 kV and a beam current of 1 mA. X-ray photoelectron spectroscopy (XPS) analyses were conducted with a K-Alpha 1063 (Thermo Fisher Scientific, USA) spectrometer using Al Kα radiation (1486.6 eV). The C 1s signal of contaminant carbon (BE = 284.6 eV) was taken as a reference for BE calibration. The specific surface areas and pore size distributions were measured on a Tristar 3000 instrument by the Brunauer–Emmett–Teller (BET) and Saito–Foley (SF) method, respectively. The element analysis was carried out using ICP-AES (IRIS1000).

2.4. Catalyst evaluation

All reactions were carried out in a three-necked round-bottom flask equipped with a reflux condenser, and the experimental setups are similar to those of our previous work.[21] Oxygen was introduced at atmospheric pressure into the solution at a desired flow rate, and the flask with a magnetic stirrer was placed in an isothermal paraffin oil bath. After the reaction, the catalyst was removed by centrifugation. The products were dissolved in acetonitrile and qualitatively analyzed by GC/MS (6890N/5973N) using an Agilent HP-5MS capillary column (30 m × 0.45 mm × 0.8 μm). For quantitative determination, the collected liquid products were analyzed on an Agilent 7820A GC with FID and an Agilent AB-FFAP capillary column (30 m × 0.25 mm × 0.25 μm). The internal standard method was employed with biphenyl being the standard.

3. Results and discussion

3.1. Catalyst characterization

The XRD patterns of the M–Z (*x*), M/Z (2.0 wt%) and regenerated M–Z (48)-1 after the first cycle of reusability test are shown in Fig. 1. They show typical MFI-type structure and the peaks match those of ZSM-5. There were no detections of peaks assignable to metal or metal oxide, suggesting that the Mn entities are either well dispersed as amorphous species or aggregated into minicrystals that are too small (<4 nm) to be detected by XRD.[24,25] Comparing the XRD patterns with that of ZSM-5 zeolite, one can see that there are diffraction peaks of M–Z (*x*) that are slightly shifted to a smaller angle. This is likely

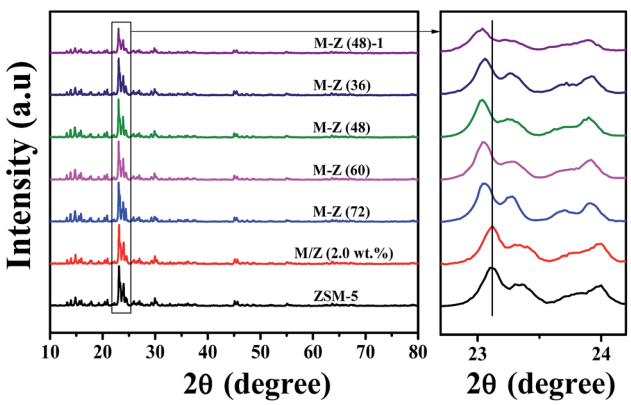

Fig. 1 XRD patterns of ZSM-5, M–Z (*x*), M/Z (2.0 wt%) and regenerated M–Z (48)-1 after the first cycle of reusability test.

to be due to isomorphous substitution of Si by Mn(II or III) that are larger in size (0.5–1.0 Å). Furthermore, there is no obvious difference between the patterns of fresh and regenerated catalysts after the first cycle of reusability test. It is hence deduced that there is no long-range change in catalyst structure during the reaction.

We examined the ZSM-5 and Mn-modified ZSM-5 samples by SEM (Fig. 2). They are all in the form of intergrown hexagonal platelets with particle size of 200–300 nm. The surface of M–Z (48) is smooth whereas that of M/Z (2.0 wt%) is decorated with small particles. To determine the surface atomic concentration and to characterize the oxidation states of surface Mn, XPS tests were carried out. The actual percentages of Mn were obtained by ICP analysis (Fig. 3). The atomic weight percentage of Mn in the M–Z (48) and M/Z (2.0 wt%) samples is 1.7 and 1.5 wt% respectively. The results are slightly less than the respective nominal values. Such discrepancy could be owing to the loss of Mn species during the centrifugation and/or stirring processes. As shown in Table 1, M/Z (2.0 wt%) and M–Z (48) have similar Mn loading, while the surface Si/Mn of M–Z (48) is only half that of the M/Z (2.0 wt%), indicating Mn accumulates on the surface of M/Z (2.0 wt%). As seen from Fig. 3, M–Z (48) and M/Z (2.0 wt%) both show a variety of Mn oxidation states that is essential for electron transfer in a material.[20,26]

Preliminary studies on the distribution of manganese species on the catalysts were conducted by means of UV-vis DRS (Fig. 4). It is generally accepted that manganese species in ZSM-5 display a number of UV-vis bands: (i) 220–380 nm ascribable to $O^{2-} \rightarrow Mn^{3+}$ charge-transfer transition or $O^{2-} \rightarrow Mn^{2+}$ charge-transfer transition, (ii) 380–600 nm attributable to isolated or extra-framework Mn^{3+} species, and (iii) above 600 nm due to manganese oxide aggregates on the external crystal surface.[14,18,27–29] Without the modification of manganese, ZSM-5 has no absorption in the 200–800 nm range. In the case of M–Z (*x*), there is absorbance at 265 nm together with a small feature at 500 nm. The latter indicates the presence of Mn(III) sites of an elongated tetragonal or distorted octahedron system.[14] It is clear that with Si/Mn increases from 72 to 48, absorption at 500 nm increases proportionally. The M/Z (2.0 wt%) sample only shows an absorption band around 250 nm with a tail extending to 800 nm, plausibly due to the existence of Mn and Mn oxide clusters on the external surface of zeolite.

Fig. 5 illustrates the nitrogen adsorption–desorption isotherms and micropore (SF method) size distribution of the

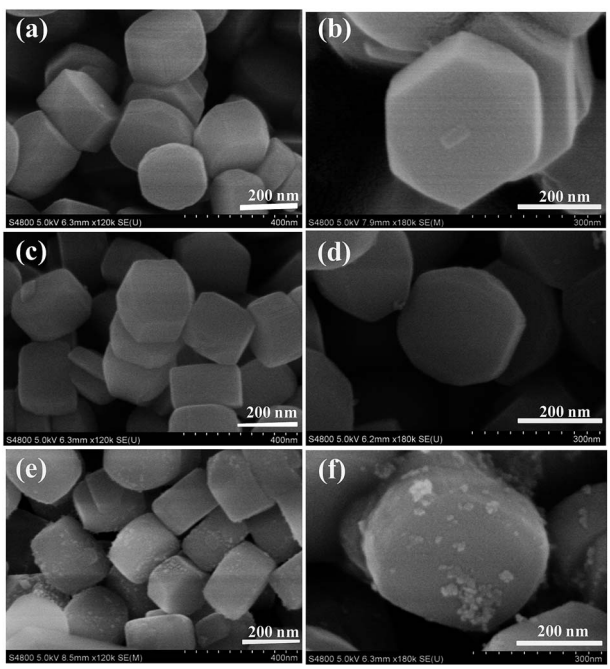

Fig. 2 SEM images of ZSM-5 (a and b), M–Z (48) (c and d) and M/Z (2.0 wt%) (e and f).

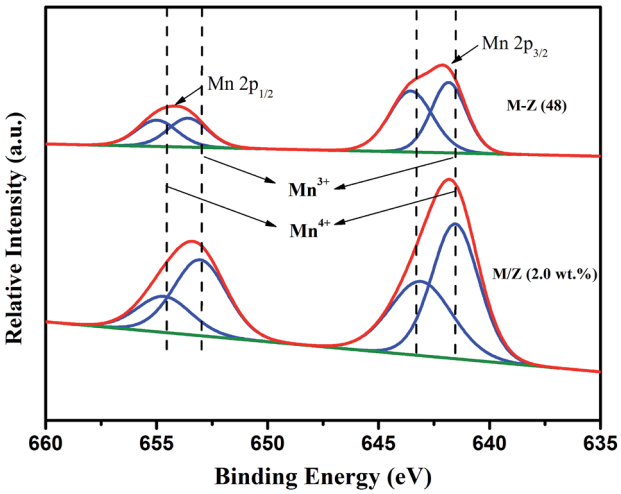

Fig. 3 XPS analysis of M–Z (48) and M/Z (2.0 wt%).

Table 1 Element composition of M–Z (48) and M/Z (2.0 wt%)

Sample	XPS Si/Mn	Mn concentration by ICP (wt%)
M–Z (48)	54.9	1.7
M/Z (2.0 wt%)	21.5	1.5

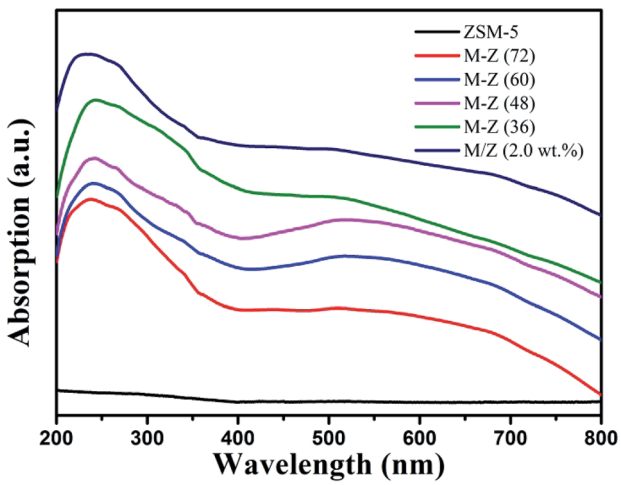

Fig. 4 UV-vis patterns of ZSM-5, M–Z (*x*) and M/Z (2.0 wt%).

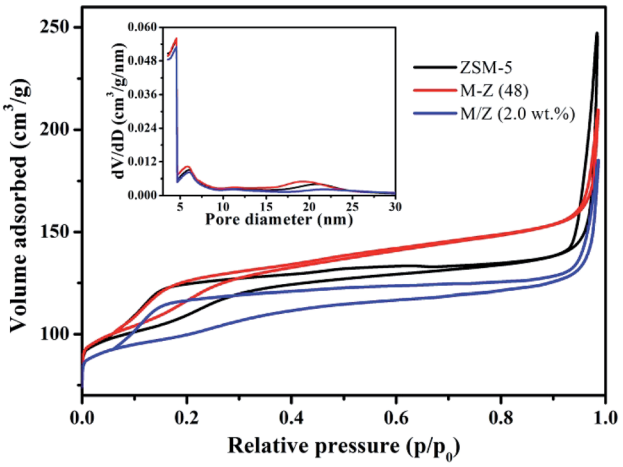

Fig. 5 N_2 adsorption–desorption isotherm and pore diameter distribution of ZSM-5, M–Z (48) and M/Z (2.0 wt%).

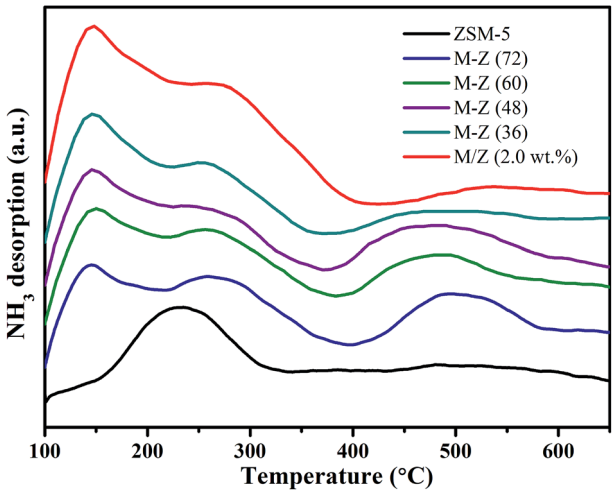

Fig. 6 NH_3-TPD profiles of as-prepared ZSM-5, M–Z (72), M–Z (60), M–Z (48), M–Z (36), M/Z (2.0 wt%).

Table 2 Textural properties of Mn-containing ZSM-5 materials

Sample	BET surface area (m^2 g^{-1})	Microporous volume (cm^3 g^{-1})	Total pore volume (cm^3 g^{-1})
ZSM-5	373.0	0.14	0.3943
M–Z (72)	375.4	0.14	0.3360
M–Z (60)	373.8	0.14	0.3384
M–Z (48)	396.2	0.14	0.3349
M–Z (36)	393.9	0.12	0.2953
M/Z (2.0 wt%)	334.5	0.12	0.2969

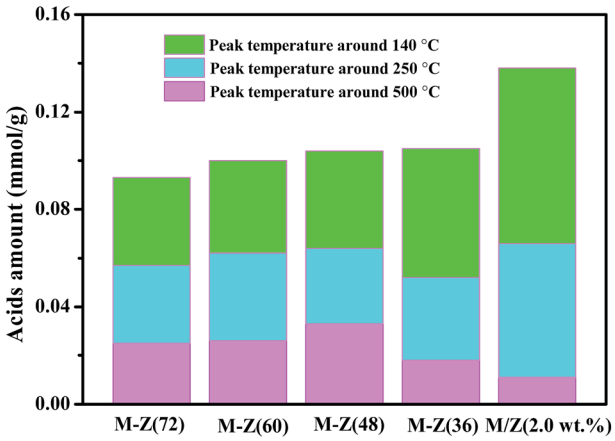

Fig. 7 Acidity distribution of catalysts measured by NH_3-TPD.

catalysts. The textural parameters are summarized in Table 2. All samples show a type-I isotherm typical of microporous materials, and the isotherms exhibit a hysteresis loop at P/P_0 of 0.1–1.0, indicating the presence of slit-shaped pores.[30] The pore size distribution curves suggest structures of uniform molecular-scale pores. Meanwhile, the total pore volume of M–Z (x) is smaller than that of ZSM-5, indicating that there is pore blockage and narrowing as a result of Mn deposition at the pore entrance and/or on the channel walls.[31] However, in the cases of M–Z (x = 72, 60, 48), the total pore volume and micro-pore volume are rather similar. It is deduced that using the hydrothermal synthesis method, there is homogeneous substitution of Mn to Si at Si/Mn molar ratio of 72, 60 and 48. With Mn dispersed in the framework throughout the materials, there is little change in pore volume. Nonetheless, the pores of M–Z (36) and M/Z (2.0 wt%) are severely blocked and narrowed as a result of excess Mn species that are scattered on the catalyst surface and inside the channels.

The acidic properties of M–Z (x) were studied to prove the intrinsic acidity caused by the incorporation of Mn. The results are shown in Fig. 6, and quantitative data of the amount of ammonia desorbed from selected samples are reported in Fig. 7. The M–Z (x) samples show two desorption peaks, one due to weak acidic sites appears as a broad peak at 140 °C with a shoulder at 240 °C, and the other due to strong acidic sites that centre at about 500 °C. The amount of ammonia desorption around 140 °C increases with the decline of Si/Mn ratio. The weak acidic sites on M–Z (x) or M/Z is related to the amount of external or extra-framework manganese ions that engender sites of weak acidity in the form of $(Mn)_nOH$, similar to those of Al_nOH groups but much weaker in strength.[32] The amount of strong acidic sites decreases in the sequence of M–Z (48) > M–Z (60) > M–Z (72) > M–Z (36). Sample M–Z (48) has the largest amount of weak acidic sites mainly because of the abundance of Mn ions in the framework, giving sites such as Mn–OH–Si and Mn···(OH)–Si with Brönsted acidity.[33] Overall, the total amounts of accessible acid sites in all the samples are relatively low.

3.2. Catalytic performance

Table 3 depicts the PCT conversion and PCB selectivity detected over the catalysts. In a blank run (without a catalyst) or over ZSM-5, there is no reactivity. However, the Mn-modified ZSM-5 catalysts perform well, confirming that catalytic activity is a result of Mn presence in the ZSM-5 zeolite. There is an increase of catalytic activity with increase of Mn loading up to Si/Mn =

Table 3 Results of *p*-chlorotoluene oxidation over different catalysts[a]

Entry	Catalyst	Conv. (%)	PCB[b]
1	No catalyst	0	0
2	ZSM-5	0	0
3	M–Z (72)	49.7	86.9
4	M–Z (60)	71.5	87.9
5	M–Z (48)	93.8	90.5
6	M–Z (36)	91.8	82.0
7	M/Z (2.0 wt%)	80.3	76.9

[a] Reaction conditions: catalyst 20 mg, *p*-chlorotoluene 1 mL, solvent (acetic acid) 10 mL, HBr (40 wt%) 30 mg, H_2O 3 g, oxygen flow rate 50 mL min^{-1}, time 8 h, temperature 110 °C. [b] PCB: *p*-chlorobenzaldehyde.

48. Further increase of Mn loading results in the decrease of PCT conversion and PCB selectivity, plausibly due to reduced Mn incorporation and/or plugging of pores that are caused by an excess amount of Mn. To investigate the effect of the distribution of active sites, the physical–chemical properties and catalytic activity of M/Z (2.0 wt%) and M–Z (48) of similar Mn loading were studied.

According to the BET results, the ZSM-5 zeolite shows high surface specific area and uniform micropores structure. The well dispersed Mn active sites on ZSM-5, as indicated in XRD analysis, should significantly enhance the catalytic activity for PCT oxidation.[21] As shown in Table 3, the PCT conversion over M–Z (48) (93.8%) is significantly higher than that over M/Z (2.0 wt%) (80.3%). With the insertion of Mn into the ZSM-5 framework, there is weakening of Mn–O bonds and enhanced amount of lattice defects.[34] Hence, besides being higher in specific surface area (396.2 m^2 g^{-1} compared to 334.5 m^2 g^{-1}), M–Z (48) is also a better oxygen carrier and donor.

With the increase of Mn active sites, there is significant improvement of PCT conversion and PCB selectivity. It is deduced that the scattering of Mn active sites in the pores of the nanoscale zeolite framework, as in the case of M–Z (48), is beneficial for the enhancement of PCB selectivity. With the mechanism suggested by Partenheimer,[22,35] bromide is directly bonded to manganese for reaction initiation. Then the oxidation of PCT in the catalyst channels leads to direct formation of benzylic bromide. Therefore, compared to those on the external surface, the active sites in the channels of a catalyst are more beneficial to PCB selectivity. However, in comparison to M–Z (48) (conv.% = 93.8, sel.% = 90.5), there is a decrease of PCB selectivity and yield over M–Z (36) (conv.% = 91.8, sel.% = 82.0). Taking the NH_3-TPD results into account, a higher content of Mn means a higher amount of both strong and weak acid sites. However, a further increase of Mn content gives rise to a decline of strong acid sites but an increase of total acid sites. In other words, excess Mn species that are scattered on the catalyst surface results in rise of the amount of weak acid sites that enhance further oxidation of PCB to carboxylic acid. In general, the high-silica MFI ZSM-5 samples are extremely low in acidity and the amounts of total acidic sites on M–Z (*x*) are approximately 0.1 mmol g^{-1}. The low external surface acidity is favourable for the partial oxidation of PCT.[21]

3.3. Effect of reaction conditions

3.3.1. Effect of catalyst amount. Fig. 8 describes the effect of catalyst amount on PCT reaction over M–Z (48). When the amount of catalyst is increased from 0 to 20 mg, there is a steep increase in PCT conversion and a slight decrease in PCB selectivity. Further increase of catalyst amount does not result in any significant changes. The results indicate that even with the enrichment of M–Z (48), only a small amount of the catalyst is utilized.[3] At the same time, the conversion of PCT is also limited by the availability of dissolved oxygen.[36] Based on the results, the amount of catalyst for optimum production of PCB should be 20 mg.

3.3.2. Effect of water addition. The effect of water addition on PCT conversion is displayed in Fig. 9. With the increase of water from 0 to 3 g, there is a significant increase of PCT conversion and PCB selectivity. As shown in Scheme 1, there is the rapid formation of *p*-chlorobenzylic bromide intermediate and its decomposition for the progress of the reaction is enhanced by water (step (1)). Furthermore, water could show other positive effects such as acting as a deactivator for the production of aromatic acids.[37] When water is in excess, the concentration of active water decreases due to self-association, and there is decline in radical production and diminution of overall reaction rate.[19] It is clear that a proper amount of water can promote the oxidation of PCT whereas in excess the oxidation reaction is inhibited. Taking PCB yield into consideration, the most suitable initial amount of water for the present reaction system should be 3 g.

3.3.3. Effect of HBr amount. The amount of HBr is a crucial factor that affects the oxidation reaction (Fig. 10). In the absence of HBr, the auto-oxidation of PCT is not significant. However, when the amount of HBr (40 wt%) is increased from 10 to 30 mg, there is a remarkable increase of PCT conversion from 33.7% to 93.8%. The attack of bromine radicals toward methyl hydrogen is a key step for reaction promotion. This facilitates

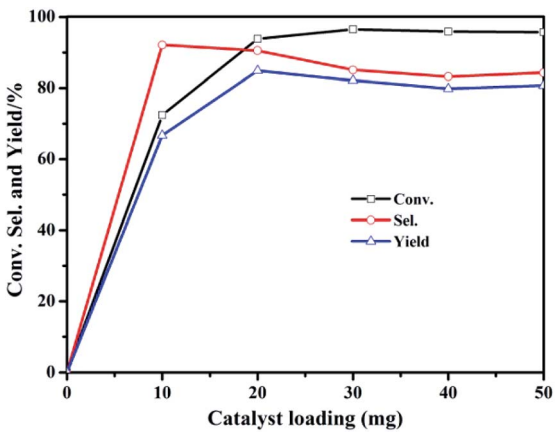

Fig. 8 Effect of catalyst amount on PCT oxidation (reaction conditions: substrate 1 mL, solvent 10 mL, HBr (40 wt%) 30 mg, H_2O 3 g, oxygen flow rate 50 mL min^{-1}, time 8 h, temperature 100 °C).

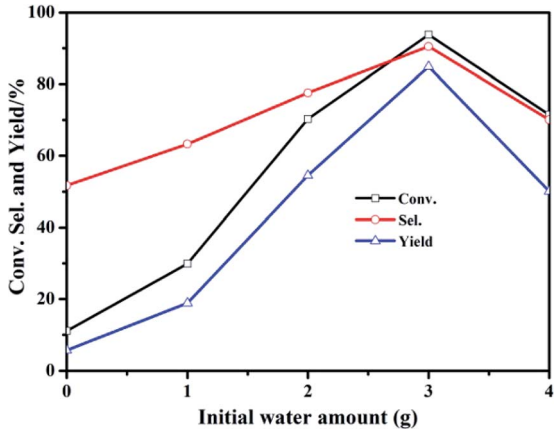

Fig. 9 Effect of water addition on PCT oxidation (reaction conditions: catalyst M–Z (48) 20 mg, substrate 1 mL, HBr (40 wt%) 30 mg, solvent 10 mL, oxygen flow rate 50 mL min^{-1}, time 8 h, temperature 100 °C).

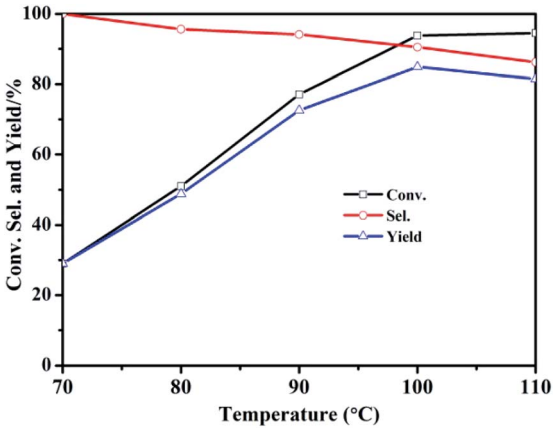

Fig. 11 Effect of temperature on PCT oxidation (reaction conditions: catalyst M–Z (48) 20 mg, substrate 1 mL, HBr (40 wt%) 30 mg, H_2O 3 g, solvent 10 mL, oxygen flow rate 50 mL min^{-1}, time 8 h).

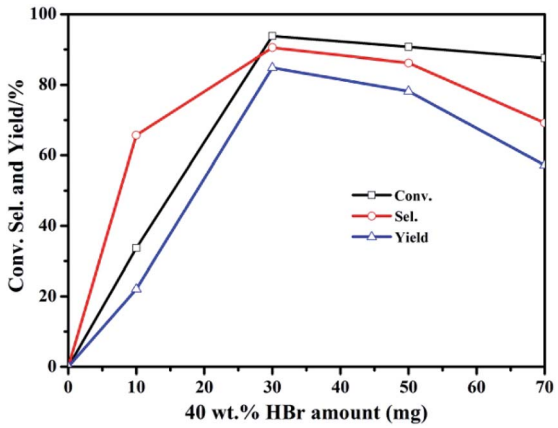

Fig. 10 Effect of HBr amount on PCT oxidation (reaction conditions: catalyst M–Z (48) 20 mg, substrate 1 mL, solvent 10 mL, H_2O 3 g, oxygen flow rate 50 mL min^{-1}, time 8 h, temperature 100 °C).

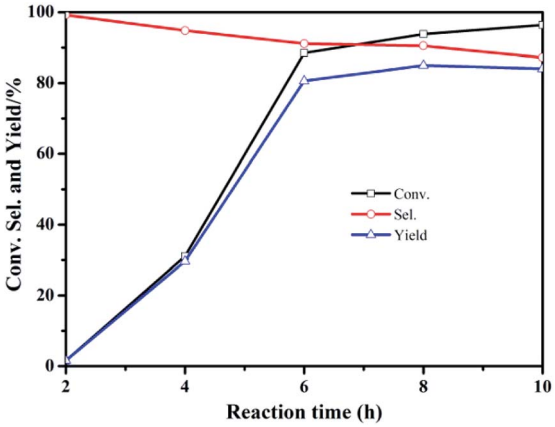

Fig. 12 Effect of reaction time on PCT oxidation (reaction conditions: catalyst M–Z (48), substrate 1 mL, solvent 10 mL, HBr (40 wt%) 30 mg, H_2O 3 g, oxygen flow rate 50 mL min^{-1}, temperature 100 °C).

electron transfer and radical formation.[2] However, an excessive amount of bromide results in an obvious decrease of conversion and selectivity. It was pointed out by Hu[38] that bromide in excess results in the formation of inactive organic bromide as well as metal–multibromides that are active for further oxidation of aldehydes.[39]

3.3.4. Effect of reaction temperature. The influence of reaction temperature on the conversion of PCT was investigated (Fig. 11). It was found that the reaction is highly sensitive to the change of temperature. Below 70 °C, the conversion of substrate is insignificant. At a higher temperature, there is a large increase of PCT conversion together with a slight decline in PCB selectivity, and PCB yield (85.0%) reaches maximum at 100 °C. The slight decrease of selectivity is attributed to the further oxidation of PCB.[3] Besides, considering the boiling point of substrate in the reaction system, the reaction temperature should be controlled at 100 °C.

3.3.5. Effect of reaction time. The effect of reaction time on PCT reaction over Mn–ZSM-5 was investigated and the results are depicted in Fig. 12. There is a significant increase in PCT conversion between 4 and 6 h. It is deduced that fierce interaction of Mn active sites with bromide results in enhancement of free radicals, and the reaction is greatly stimulated. Under the adopted condition, PCT conversion increases to 96.4% in 10 h, while there is a constant decrease in PCB selectivity. Based on the results, we consider that 8 h is the reaction time for optimal performance.

3.4. Recycling of the catalyst

Recyclability of the catalysts for liquid-phase oxidation of PCT was tested. After each cycle, the catalyst was filtered out and washed several times with acetone or anhydrous alcohol before being dried at 120 °C overnight. Listed in Table 4 are the results. M–Z (48) shows an immediate decrease of activity after the first cycle. However, after successive recycling (cycles 2 to 4) of the catalyst, there is a minor decrease in catalytic activity. Although there was slight fading of colour after each cycle, the XRD pattern of a recovered catalyst (Fig. 1) is similar to that of the

Table 4 The recycling of M–Z (48) in the oxidation of *p*-chlorotoluene[a]

Recycle number	1 (fresh)	2	3	4
Conv. (%)	93.8	82.1	79.5	80.2
Sel. (%)	90.5	96.4	95.8	95.1

[a] Reaction conditions: catalyst 20 mg, *p*-chlorotoluene 1 mL, solvent (acetic acid) 10 mL, HBr (40 wt%) 30 mg, H_2O 3 g, oxygen flow rate 50 mL min^{-1}, time 8 h, temperature 110 °C.

fresh one, indicating that there is no change in catalyst structure. In other words, the deactivation of catalyst is likely to be due to the leaching of a small amount of manganese from the catalyst during reaction. It is observed that the leaching of manganese decreases in further cycles. Therefore, catalytic activity probably originates from the manganese ions in the framework of M–Z (*x*). The results indicate that the catalyst can be recycled a number of times without showing significant loss of catalytic activity.

4. Conclusions

Efficient synthesis of *p*-chlorobenzaldehyde by liquid-phase oxidation of *p*-chlorotoluene with molecular oxygen was achieved over Mn–ZSM-5 (Si/Mn = 48, Mn 1.7 wt%) under optimized conditions (catalyst 20 mg, *p*-chlorotoluene 1 mL, solvent (acetic acid) 10 mL, HBr (40 wt%) 30 mg, H_2O 3 g, oxygen flow rate 50 mL min^{-1}, time 8 h, temperature 100 °C). With 93.8% *p*-chlorotoluene conversion and 90.5% *p*-chlorobenzaldehyde selectivity, the highest product yield is 85.4%. It is shown that the Mn active sites resulted from manganese incorporation into the ZSM-5 framework play an effective role in *p*-chlorotoluene oxidation. The superior performance of the Mn–ZSM-5 catalyst is attributed to its mild acidity and good distribution of manganese species.

Acknowledgements

The project was financially supported by the National Natural Science Foundation of China (Grant No. 21476065, 21273067), the program for New Century Excellent Talents in Universities (NCET-10-0371), Program for Changjiang Scholars and Innovative Research Team in University (IRT1238), and the Fundamental Research Funds for the Central Universities. C. T. Au thanks the Hunan University for an adjunct professorship.

References

1 R. A. Sheldon and H. V. Bekkum, *Fine Chemicals through Heterogeneous Catalysis*, Wiley-VCH, Weinheim, 2001.
2 A. J. Hu, C. X. Lü, H. Y. Wang and B. D. Li, *Catal. Commun.*, 2007, **8**, 1279–1283.
3 J. Q. Wang, H. Fang, Y. Li, J. J. Li and Z. Y. Yan, *J. Mol. Catal. A: Chem.*, 2006, **250**, 75–79.
4 F. M. Bautista, D. Luna, J. Luque, J. M. Marinas and J. F. Sánchez-Royo, *Appl. Catal., A*, 2009, **352**, 251–258.
5 N. N. Tušar, S. Jank and R. Gläser, *ChemCatChem*, 2011, **3**, 254–269.
6 J. S. Yoo, *Appl. Catal., A*, 1996, **135**, 261–271.
7 C. Sprung and B. M. Weckhuysen, *Chem.–Eur. J.*, 2014, **20**, 3667–3677.
8 H. X. Tao, H. Yang, X. H. Liu, J. W. Ren, Y. Q. Wang and G. Z. Lu, *Chem. Eng. J.*, 2013, **225**, 686–694.
9 H. L. Janardhan, G. V. Shanbhag and A. B. Halgeri, *Appl. Catal., A*, 2014, **471**, 12–18.
10 D. B. Shah, D. T. Hayhurst, G. Evanina and C. J. Guo, *AIChE J.*, 1988, **34**, 1713–1717.
11 W. Tan, M. Liu, Y. Zhao, K. K. Hou, H. Y. Wu, A. F. Zhang, H. O. Liu, Y. R. Wang, C. S. Song and X. W. Guo, *Microporous Mesoporous Mater.*, 2014, **196**, 18–30.
12 Y. T. Cheng, Z. Wang, C. J. Gilbert, W. Fan and G. W. Huber, *Angew. Chem., Int. Ed.*, 2012, **51**, 11097–11100.
13 Q. Ouyang, S. F. Yin, L. Chen, X. P. Zhou and C. T. Au, *AIChE J.*, 2013, **59**, 532–540.
14 D. Radu, P. Glatzel, A. Gloter, O. Stephan, B. M. Weckhuysen and F. M. F. de Groot, *J. Phys. Chem. C*, 2008, **112**, 12409–12416.
15 Y. Chen, G. Li, F. Yang and S. M. Zhang, *Polym. Degrad. Stab.*, 2011, **96**, 863–869.
16 G. Lv, F. Bin, C. L. Song, K. P. Wang and J. O. Song, *Fuel*, 2013, **107**, 217–224.
17 X. R. Lou, P. F. Liu, J. Li, Z. Li and K. He, *Appl. Surf. Sci.*, 2014, **307**, 382–387.
18 Y. T. Meng, H. C. Genuino, C. H. Kuo, H. Huang, S. Y. Chen, L. C. Zhang, A. Rossi and S. L. Suib, *J. Am. Chem. Soc.*, 2013, **135**, 8594–8605.
19 Y. Q. Deng, T. Zhang, C. T. Au and S. F. Yin, *Appl. Catal., A*, 2013, **467**, 117–123.
20 Y. Q. Deng, T. Zhang, C. T. Au and S. F. Yin, *Catal. Commun.*, 2014, **43**, 126–130.
21 T. Zhang, Y. Q. Deng, W. F. Zhou, C. T. Au and S. F. Yin, *Chem. Eng. J.*, 2014, **240**, 509–515.
22 W. Partenheimer, *Adv. Synth. Catal.*, 2004, **346**, 297–306.
23 E. M. Flanigen, J. M. Bennett, R. W. Grose, J. P. Cohen, R. L. Patton and R. M. Kirchner, *Nature*, 1978, **271**, 512–516.
24 H. X. Yuan, Q. H. Xia, H. J. Zhan, X. H. Lu and K. X. Su, *Appl. Catal., A*, 2006, **304**, 178–184.
25 H. H. Chen, H. P. Zhang and Y. Yan, *Chem. Eng. J.*, 2014, **254**, 133–142.
26 L. Wang, H. P. Zhang, Y. Yan and X. Y. Zhang, *RSC Adv.*, 2015, **5**, 29482–29490.
27 F. Milella, J. M. Gallardo-Amores, M. Baldic and G. Busca, *J. Mater. Chem.*, 1998, **8**, 2525–2531.
28 S. Velu, N. Shah, T. M. Jyothi and S. Sivasanker, *Microporous Mesoporous Mater.*, 1999, **33**, 61–75.
29 B. Qi, X. H. Lu, D. Zhou, Q. H. Xia, Z. R. Tang, S. Y. Fang, T. Pang and Y. L. Dong, *J. Mol. Catal. A: Chem.*, 2010, **322**, 73–79.
30 B. J. Dou, G. Lv, C. Wang, Q. L. Hao and K. S. Hui, *Chem. Eng. J.*, 2015, **270**, 549–556.
31 G. Q. Zhou, J. Li, Y. Q. Yu, X. G. Li, Y. J. Wang, W. Wang and S. Komarneni, *Appl. Catal., A*, 2014, **487**, 45–53.

32 J. C. Xia, D. S. Mao, B. Zhang, Q. L. Chen and Y. Tang, *Catal. Lett.*, 2004, **98**, 235–240.
33 G. Centi, S. Perathoner and F. Trifirb, *J. Phys. Chem.*, 1992, **96**, 2617–2629.
34 R. H. Wang and J. H. Li, *Environ. Sci. Technol.*, 2010, **44**, 4282–4287.
35 W. Partenheimer, *J. Mol. Catal. A: Chem.*, 2001, **174**, 29–33.
36 A. R. Li, S. W. Tang, P. H. Tan, C. J. Liu and B. Liang, *J. Chem. Eng. Data*, 2007, **52**, 2339–2344.
37 W. Partenheimer, *Catal. Today*, 1995, **23**, 69–158.
38 A. J. Hu, C. X. Lü, B. D. Li and T. Huo, *Ind. Eng. Chem. Res.*, 2006, **45**, 5688–5692.
39 W. Partenheimer, *J. Mol. Catal. A: Chem.*, 2003, **206**, 105–119.